RSC Advances

ROYAL SOCIETY OF CHEMISTRY

www.rsc.org/advances

Table of content

Synthesis of a novel bifunctional nanocomposite with tunable upconversion emission and magnetic properties

Qian Cheng,[a,b] Yu Li [c], Shouxin Liu [a]*,Jiehe Sui,[b] and Wei Cai [b]

A method of Co^{2+} ions codoping for significantly enhancing upconversion emission intensity and simultaneous controlling sparamagnetic properties in β-$NaYF_4$: Yb/Er nanoparticles, with well maintaining their morphology and highly disperse.

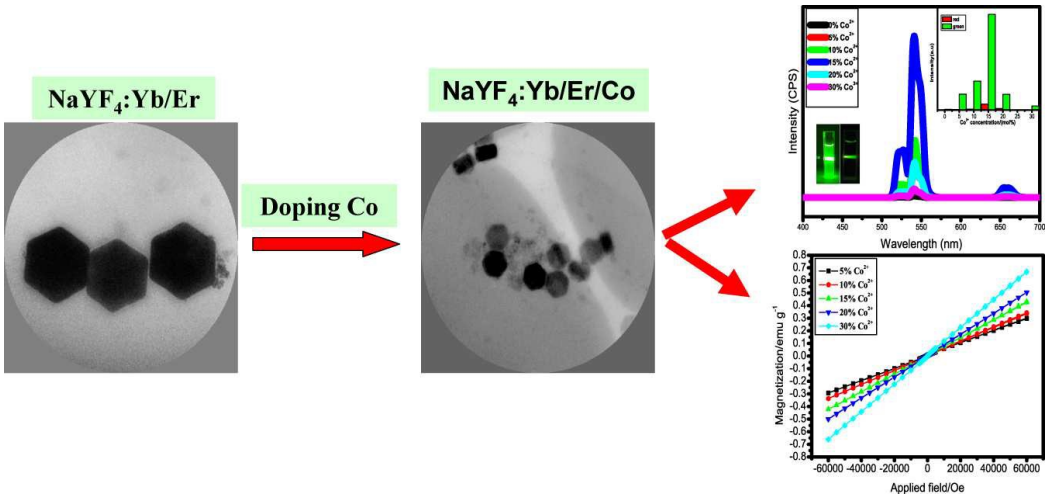

RSC Advances

PAPER

Synthesis of a novel bifunctional nanocomposite with tunable upconversion emission and magnetic properties

Received 00th January 20xx,
Accepted 00th January 20xx

DOI: 10.1039/x0xx00000x

www.rsc.org/ Advances

Qian Cheng,[a, b] Yu Li,[c] Shouxin Liu,[a]* Jiehe Sui[b], and Wei Cai[b]

Fluorescent and magnetic bifunctional $NaYF_4$:Yb/Er/Co nanoparticles were synthesized for the first time via a thermalysis method using oleic acid as capping ligand and octadecene as solvent. The effect of Co^{2+}-codoped on the size evolution, crystal structure, UC emission and magnetic properties of $NaYF_4$:Yb/Er nanoparticles was investigated in detail. XRD, EDS and XPS measurements revealed that Co^{2+} ions had been successfully incorporated into $NaYF_4$ matrix and existed in the host lattice under the II valence state. The different concentration of Co ions codoping did not change the structure of hexagonal phase. However, the green and red upconversion(UC) emissions intensity of hexagonal $NaYF_4$:Yb/Er were obviously strengthened by tridoping the structure with Co^{2+}/Yb^{3+}/Er^{3+}, and the decay time was obviously prolonged with different quantity of Co^{2+} ions tridoping. The luminescence enhancement should be attributed to the distortion of the local asymmetry around Er^{3+} ions. A possible mechanism for the enhancement of upconversion emission was discussed. More importantly, owing to the cobalt ion doping, the $NaYF_4$ nanoparticles also present paramagnetic properties at room temperature and superparamagnetic properties at low temperature. Therefore, it is expected that these nanocrystals can be used as promising dual-modal nanoprobes for optical bioimaging and magnetic resonance imaging (MRI), and may have potential applications in bioseparation.

1. Introduction

Trivalent lanthanide (Ln^{3+}) ions-doped luminescent nanoparticles(NPs) have attracted much attention and come to the forefront in nanophotonics owing to their superior optical features including large effective Stoke shifts, sharp emission bandwidths, long photoluminescence(PL) lifetime, low toxicity as well as high resistance to photo bleaching. [1-3] These unique properties make them highly suitable for use as alternatives to organic fluorescent dyes or quantum dots (QDs) for various biological applications. Among these materials, hexagonal (β) $NaYF_4$ NPs has been reported to be the most effective host material for UC emission due to its intrinsic low phonon energies (~350cm^{-1}), which decreases the nonradioactive relaxation probability and results in more efficient UC emissions. [4, 5] Up to now, lots of research has focused on the study of β-$NaYF_4$ NPs.[6-8] Despite significant progress in studying the bioapplication of UCNPs, the low emission efficiency of UCNPs limits the practical application for in vivo imaging[9-11]. Recently, some reports on incorporating atoms or ions of appropriate elements into host lattices to yield hybrid materials with desirable properties and functions have attracted wide attention of researches. For example, Liu X.G etc reported that doping of lanthanide ions with a size larger than Y^{3+} in $NaYF_4$ host lattices could dominate the formation of pure hexagonal-phase $NaYF_4$ NPs. Furthermore, they had successfully fulfilled to synthesize upconversion NPs with simultaneous controlling over crystal phase, size and emission colours through the control different combinations of lanthanide dopants at precisely defined concentration.[12] Very recently, Hao's group reported that Gd^{3+} codoped $NaLuF_4$:Yb^{3+}/Tm^{3+} NPs with near-infrared upconversion and magnetic properties could be readily modified by doping with Gd^{3+} and demonstrated that Gd^{3+} addition could promote the transformation from the cubic to hexagonal phase and reduced the size.[13]

Transition metal(TM) ions such as iron, cobalt, manganese and molybdenum ions codoping into some host lattices can also generate magnetic properties or modify the structure, size and optical properties.[14-16] For example, cobalt and nickel ions doped into ZnO NPs could giving them different optical and magnetic properties.[14] Furthermore, Co doping could effectively adjust the energy level in ZnO nanorods, which led to variation in the UV emission peak position and enhanced the luminescence performance in the visible light region as well modify ZnO NPs with magnetic properties.[15] However, rarely applied on UCNPs, furthermore, size, shape and phase have great influence on their luminescence and biological application. Wu's group reported incorporating 10mol%Mo^{3+} ions into $NaYF_4$:Yb^{3+},Er^{3+} nanoparticles could enhance the

[a] School of Materials Science and Engineering, Northeast Forestry University, Harbin 150040, PR China.E-mail:liushouxin@126.com;Tel(+86)451-8219-1502; Fax:(+86)451-8219-1506.
[b] National Key laboratory of Materials Behaviours &Evaluation Technology in Space Environments , Harbin Institute of Technology, Harbin, 150001, PR China.
[c] College of Science, Northeast Forestry University, Harbin 150040, P. R. China.
† Electronic Supplementary Information (ESI) available: [*X-ray diffraction data, XPS and EDS, M(H) of the Co-doped $NaYF_4$: Yb^{3+}/Er^{3+} NPs measurements at 2 and 300K .*]. See DOI: 10.1039/x0xx00000x

intensity of green and red emission by 6 and 8 times respectively.[17] zhao's group reported that $NaYF_4$: Yb^{3+}/Er^{3+} upconversion NPs doped Mn^{2+} could make simultaneously controlling the phase and UC emission behavior.[18] Tian's group found the total luminescence intensity of $NaYbF_4:Er^{3+}$ UCNPs doped with 20mol% Mn^{2+} ions is about 20 times higher than that of $NaYbF_4:Er^{3+}$ UCNPs doped without Mn^{2+} ions[19]. J. Kim doped 30mol%Fe^{3+} in $NaGdF_4$:Yb,Er nanocrystals and observed enhancement up to 34 and 30 times in the visible green and red UC emissions.[20] All of the above results show that transition metal ions doping into the host lattice can modify the optical and magnetic properties. However, as far as we know, there is no report on the study of influence on the upconversion emission intensity and magnetic properties of $NaYF_4$:Yb,Er NPs by metal Co^{2+} ions codoping.

In this paper, we report the upconversion emission enhancement in β-$NaYF_4:Yb^{3+}/Er^{3+}$ NPs by co-doping cobalt ion. The influence of Co^{2+} ions on the crystalline structure, size, UC emission and the radiation lifetimes of intermediate $^4S_{3/2}$ and $^4F_{9/2}$ (Er) states of β-$NaYF_4:Yb^{3+}/Er^{3+}$ NPs was investigated. Furthermore the influence of Co^{2+} ions on magnetization was presented. The as-synthesized fluorescent and magnetic bifunctional $NaYF_4$:Yb/Er/Co NPs have highly efficient UC luminescence and excellent paramagnetic behaviour, which may have potential applications in bioseparation, fluorescent and MRI bioimaging.

2. Experimental

2.1 Chemicals and methods

Oleic acid (OA,90%), trifluoroacetic acid (TFA,99%), 1-octadecene (ODE,70%) and Cobalt(II) acetylacetonate ($Co(acac)_2$,98%) were purchased from Aldrich. All other chemicals were analytical grade and used without further purification. Water used in the experiment was purified to resistivity of 18.2 MΩ. RE_2O_3 (RE =Y, Yb and Er) used were of 99.99% purity. Rare-earth trifluoroacetates ($(CF_3COO)_3RE$) were prepared from the corresponding metal oxides and TFA followed by the literature method.[21]

2.2 Synthesis of Co^{2+}-doped $NaYF_4$ nanoparticles

$NaYF_4$:2%Er^{3+}/20%Yb^{3+}/xCo^{2+} (x =0%, 5%, 10%, 15%, 20% and 30%) NPs were synthesized by a modified co-thermolysis method using oleic acid as both a stabilizing and a chelating agent. The mixture of $(CF_3COO)_3Y$, $(CF_3COO)_3Yb$, $(CF_3COO)_3Er$, CF_3COONa and $Co(acac)_2$ with corresponding mole ratios was dissolved in OA (20 mL) and ODE(20 mL). Under vigorous stirring, the mixture was then heated to 110 °C under the protection of argon atmosphere and maintained at the same temperature for 30 min to remove the oxygen and residual water. Finally, the solution was totally clear with a blue colour. The resultant blue solution was then heated quickly to 330 °C in the presence of argon for protection from oxidation. After heating for 1.5 h, the transparent purple reaction mixture was cooled down to 80 °C before ethanol (20 mL) was added. The NPs were isolated by centrifugation. They were washed three times with hexane and three times with deionized water to remove the NaF residue. The resulting NPs were dried in vacuum at 50 °C for 24h.

2.3 Characterization

The crystal structure was analyzed by a Rigaku-D/max 2500 X-ray diffractometer(XRD) using a nickel-filtered Cu*Ka* radiation (λ= 0.15405 nm). The morphologies and sizes of the samples were characterized using transmission electron microscopy (TEM) images on a Philips Tencai 20 at an accelerating voltage of 200kV. The X-ray photoelectron spectra(XPS) were measured on an ESCA PHI500 spectrometer by using a twin-anode Cu *Ka*(12.5KV) X-ray source. All the spectra were calibrated to the binding energy of the adventition C1s peak at 284.6 eV. The upconversion emission spectra were acquired using FluoroMax-4 fluorescence spectrometer system equipped with a focused 1300 mW power-controllable 980 nm diode laser coupled to a 100 μm (core) fiber and the luminescent photographs were taken with Nikon D3100 digital camera. The magnetization as a function of the applied magnetism of the Co^{2+} codoped $NaYF_4:Yb^{3+}/Er^{3+}$ nanocrystals was carried out by the physical properties measurement system (PPMS) of Quantum Design with a magnetic field up to 6 T. All the measurements were performed at room temperature.

3. Results and discussion

3.1 Structure and morphology

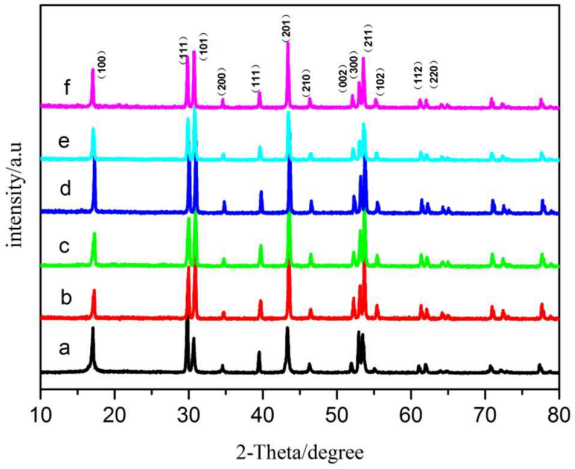

Fig. 1 XRD patterns of $NaYF_4$ samples doped with different Co^{2+} contents: (a) 0%, (b) 5%, (c) 10%, (d) 15% (e) 20% and (f) 30%.

The phase and morphology of the as-prepared samples were analyzed by XRD and TEM techniques, respectively. Fig.1 shows the XRD patterns of the $NaYF_4$ doped with 2 mol% Er^{3+}, 20 mol %Yb^{3+} ions, and tridoped with different concentrations of Co^{2+} ions. As shown in Fig.1, all the peak positions and intensities match closely with those of hexagonal structure according to Powder Diffraction File PDF 16-0334. In addition, no other impurity diffraction peaks were observed even the Co^{2+} ions concentration increased to 30 mol%, indicating all the Co^{2+} ions were incorporated into the host matrix and formed a Y-Co solid solution structure. The XPS survey

Table1 the lattice constants and unit-cell volumes of $NaYF_4$:Yb/Er doped with different concentrations of Co^{2+}

	0%Co^{2+}	**5%**Co^{2+}	**10%**Co^{2+}	**15%**Co^{2+}	20% Co^{2+}	**30%** Co^{2+}
a/Å	5.973	5.965	5.960	5.950	5.962	5.971
c/Å	3.510	3.498	3.494	3.500	3.504	3.505
unit-cell volume /$Å^3$	108.44	107.79	107.35	107.276	108.12	108.28

spectrum (Figure S1) shows the presence of Na, Y, F, Yb, Er and Co elements . The peak located at 781.9 eV and 795.3 eV can be attributed to the binding energy of $Co^2p_{3/2}$ and Co $^2p_{1/2}$ orbital's, respectively, which is also indicating all the Co^{2+} ions were incorporated into the host matrix and formed a Y-Co solid solution structure.

Moreover, all the diffraction peaks shift slightly to larger angles as Co^{2+} ion concentration increases from 0 to15 mol%, and then gradually move reversely for Co^{2+} ion concentration of 15-30 mol%(see supporting information Figure S2). The shifting of the peak's position shows that the lattice parameters changes with the different concentration of Co^{2+} ions codoping. The above results were shown in table.1. Owing to the substitution of Y^{3+}(radius=0.89Å) by the smaller Co^{2+} ion(radius=0.72 Å), the unit –cell volume decreases with increasing Co^{2+} content at the range of 0-15 mol%, and then increases with Co^{2+} content at the range of 15-30 mol%, this may be attributed to a change in symmetry that the cell volume of $NaYF_4$ did not decrease linearly with increasing Co^{2+} doping concentration.[21,22] This change also suggests that Co^{2+} ions with smaller ionic radii substitute or occupation of interstitial sites for Y^{3+} in the $NaYF_4$ lattice, and the unit cell contracts to accommodate these heterogeneous ions.

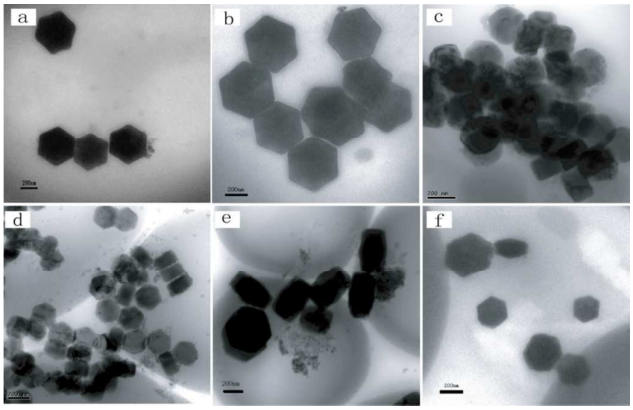

Fig. 2 TEM images of the $NaYF_4$: $20\%Yb^{3+}/1\%Er^{3+}/xCo^{2+}$ nanoparticles: (a) 0%, (b) 5%, (c) 10%, (d) 15%, (e) 20%,(f) 30%

Fig.2 shows the typical TEM images of the as-prepared $NaYF_4$ NPs doped with different contents of Co^{2+} ion. As shown in Fig.2，the nanoparticles were hexagonal nanoplate with good dispersivity, and the morphology has not been affected by codoping of Co^{2+} ions. With increasing Co^{2+} doping concentration from 15% to 20%，the size of nanoplate slightly changes small, however, the thickness of nanoplate increases, indicating that doping of Co^{2+} ions can influences the growth of crystals. The phenomenon is similar to Sn^{4+} ions codoping in $NaYF_4$ nanoparticles,[23] which attribute to organic molecules being selectively adsorbed on crystal surfaces and controling the growth rates along different directions. And EDS spectrum in Figure S2 clearly shows the presence of Co and other elements confirming the successful doping of Co and other elements.

3.2 Optical properties of the $NaYF_4$:$Yb^{3+}/Er^{3+}/Co^{2+}$ nanoparticles

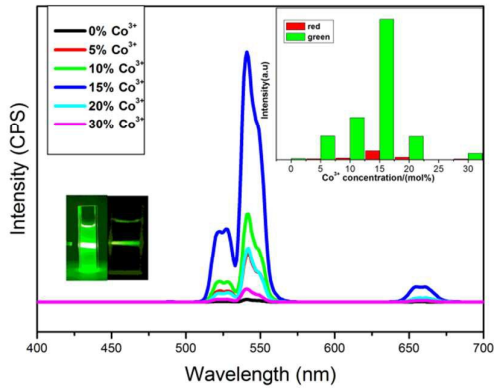

Fig.3 Upconversion luminescence spectra of $NaYF_4$: $20\%Yb^{3+}/2\%Er^{3+}/xCo^{2+}$ (x= 0%–30%). The inset of left low figure shows a digital photo of the 0.1 wt% cyclohexane solution of the as-prepared $NaYF_4$: $20\%Yb^{3+}/2\%Er^{3+}/15\%$ Co^{2+} sample under the excitation of 980 nm light with a power density of 54 W /cm^2.

To investigate the influence of different Co^{2+} tridoping concentration on UC luminescence, the room temperature upconversion luminescence spectra of $NaYF_4$: $20\%Yb^{3+}/2\%Er^{3+}/xCo^{2+}$(x =0%, 5%, 10%, 15%, 20% and 30%) NPs were measured using FluoroMax-4 fluorescence spectrometer system equipped with a focused 1300 mW power-controllable 980 nm diode laser coupled to a 100 μm (core) fiber, and were shown in Fig.3. All the samples exhibited three distinct bands in the range of 500-700 nm. According to the Fig.3, the dominant green emissions ranging from 515 to 530 nm and from 530 to 550 nm were assigned to the $^2H_{11/2} \rightarrow {}^4I_{15/2}$ and $^4S_{3/2} \rightarrow {}^4I_{15/2}$ transitions, respectively. the red emission from 635 to 670 nm was attributed to the $^4F_{9/2} \rightarrow {}^4I_{15/2}$ transition. In addition, the figure showed that the intensity of green and red UC luminescence was drastically enhanced with the increasing of Co^{2+} ions tridoping concentration, when the Co^{2+} ions concentration reached 15 mol%, the green and red UC luminescence intensity reached its maximum and were about 114 and 84 times stronger than that of Co^{2+} ions free sample, respectively. And then, the UC luminescence intensity was reduced with further increasing Co^{2+} ions tridoping concentration. The inset of Fig.3 also shows the enhancement

of green and red upconversion emissions as a function of Co^{2+} ions. The changing trend of each emission was of the same, however, the half-peak width of $^4S_{3/2} \rightarrow ^4I_{15/2}$ transitions (~543nm) emission was changed obviously with respect to the Co^{2+} doping level, and the changing trend was of the same with the change of the UC luminescence intensity, which showed that $^4S_{3/2}$ energy level and energy bandwidth had been influenced by Co^{2+} codoping. In addition, to visualize the improvement of the UC emissions, the photograph of the upconversion luminescence of as prepared $NaYF_4$: 20%Yb^{3+},2%Er^{3+},15Co^{2+} NPs(right) and $NaYF_4$:20%Yb^{3+}, 2%Er^{3+} NPs (left) solution in cyclohexane (0.1wt%) excited with a 980nm laser diode (taken by a digital camera without any additional filter) are provided in the inset of Fig3. As shown in this figure, $NaYF_4$: 20%Yb^{3+}, 2%Er^{3+},15Co^{2+} NPs exhibits good dispersion, the fluorescent strength is significantly enhanced by codoping Co^{2+} ions and the changes in fluorescent strength are clearly observed with the naked eye.

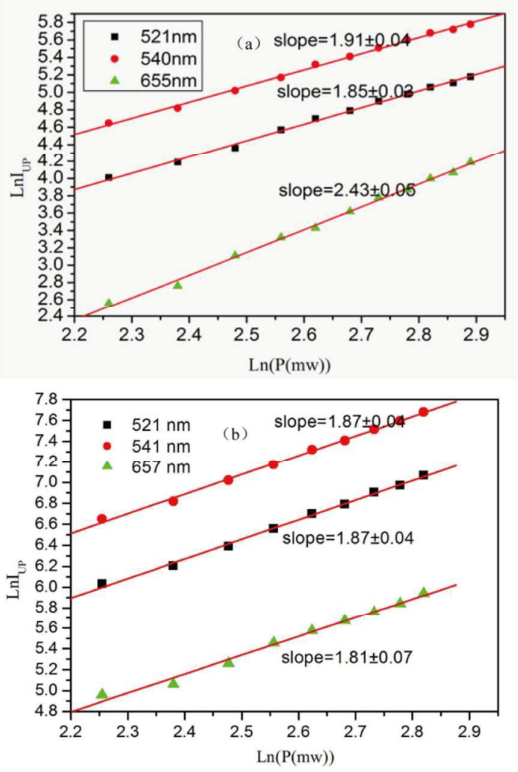

Fig. 4 Pump power dependence of the green and red emission of $NaYF_4$:Yb/Er/Co NPs: (a) 0 mol% Co^{2+} , (b)15 mol% Co^{2+}

In order to better understand the fact above, the UC luminescence intensities were measured as a function of excitation power for $NaYF_4$: Yb/Er/Co NPs codoped with 0 and 15 mol% Co^{2+} shown in Fig.4. For the unsaturated upconversion process, the number of photons required to populate the upper emitting state can be described by the following relation [22, 24]: $I_{up} \propto I_{NIR}^{n}$ Where I_{up} is the upconversion emission intensity, I_{NIR} is the pump laser intensity, and n is the number of pump photons required. As shown in Fig.4b, the slopes (n values) obtained were 1.87±0.04, 1.87±0.04 and 1.81±0.07 for 521, 541 and 657nm emissions in $NaYF_4$: Yb^{3+}/Er^{3+} sample with codoping 15 mol% Co^{2+}, which are slightly smaller than n values(1.91±0.04, 1.85±0.03 and 2.43±0.05) for $NaYF_4$:Yb^{3+}/Er^{3+} NPs (Fig.4a). These results indicate that the green and red emissions are all a two-photon processes in both nanocrystals with and without Co^{2+} ions. The Co^{2+} ions cannot absorb 980 nm photons and cannot transfer its energy to Er^{3+}, which indicates that the mechanisms for UC radiations have not been affected by introducing of Co^{2+} ions. And typical energy level for upconversion emission of $NaYF_4$:Yb^{3+}/Er^{3+} under 980nm is shown in Fig.5. The above phenomenon was different from that of Mn^{2+} doped $NaYF_4$: Yb^{3+}/Er^{3+} NPs, [21] So, the ratio of the red and green emission cannot be changed by codoping Co^{2+}, but the intensity of the green and red emission was obviously enhanced.

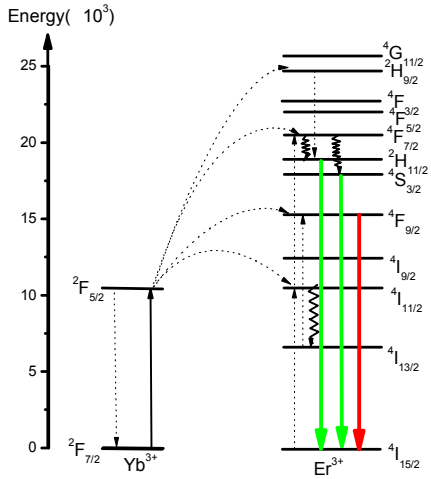

Fig 5. Energy level diagrams of the Yb^{3+} and Er^{3+} ions as well as the proposed UC mechanism for the green and red emission

Why did the UC luminescence intensity change with different Co^{2+} tridoping concentration? As well known, the upconversion luminescence intensity of rare earth is mainly dependent on electronic transition probabilities and a hypersensitive transition, however, the electronic transition probabilities are sensitively affected by the local crystal field symmetry of the Er^{3+} ions, and the hypersensitive transition can be produced by the rare earth of surrounding[25, 26]. According to the energy level diagram shown in Fig.5, when absorbing a photon, the electrons of Yb^{3+} ions on the ground state ($^2F_{7/2}$) are excited to a higher energy level ($^2F_{5/2}$), and subsequently, the energy is transferred to the adjacent Er^{3+} ions due to the energy overlap of the transition dipoles of the two elements. Finally the energy is released by Er^{3+} ions in the form of light emission and partial heat.[29-32] In this through-space interaction, the distance between the Yb^{3+} and Er^{3+} ions plays an key role. If the ions are far separated from each other, the energy transfer is not efficient. On the other hand, the closely spaced ions will lead to deleterious cross-relaxation, which decreases the emission efficiency. Thus, the

Table 2. Lifetimes of the $^4S_{3/2}$ and $^4F_{9/2}$ states of Er^{3+} ions for $NaYF_4$: Yb, Er NPs with introducing 0-30 mol% Co^{2+} ions

Co^{2+} concentration(mol%)	0	5	10	15	20	30
τ_1(ms) ($^4S_{3/2}$)	0.12	0.43	0.53	0.63	0.48	0.33
τ_2 (ms) ($^4F_{9/2}$)	0.17	0.60	0.68	0.82	0.67	0.61

fluorescence emission of the upconverison NPs is affected by the distance between the Yb^{3+} and Er^{3+} ions. Furthermore, the change in the upconversion nanocrystal lattice also affects the fluorescence emission.[5] Therefore，we deduce that the change of UC emission intensity may come from the fact that doping with a small radius of ions can change the distance between the Yb^{3+} and Er^{3+} ions by introducing different concentrations of Co^{2+} ions. It is well known that substituting of Y^{3+} (radius =0.89Å) ion by the smaller Co^{2+} ion (radius=0.72 Å) can caused the host lattice to shrink, whereas occupating the interstitial sites can cause the host lattice to expand. [28] The above shrinkage or expand as well as both of them can cause the bond length and trivalent cation space to change; Moreover, the symmetry is also caused to change. All of above changes indicate that the surrounding environment of rare hypersensitive transition, and the distance between the Yb^{3+} and Er^{3+} ions affect the electronic transition probabilities, furthermore enhance UC luminescence intensity. Therefore, the intensity of normalized decay curve of the $^4S_{3/2}\rightarrow{}^4I_{15/2}$ transition at 541nm in the samples. All the decay curves of the samples could be well fitted to a single exponential function as, $I(t)= I_0 + A_1 \exp(-t/\tau_1)$, where I and I_0 are the luminescence intensity at time t and 0. A_1 is constant, t is time, and τ_1 is the decay times for the exponential components. The lifetimes of $^4S_{3/2}$ and $^4F_{9/2}$ states of Er^{3+} ions for $NaYF_4$:Yb^{3+}/Er^{3+} NPs with introducing 0-30 mol% Co^{2+} ions were listed in Table 2. It is well known that the inverse of the lifetime is equal to the sum of the radioactive transition and nonradioactive transition. As shown in Table 2, it can be seen that all the lifetimes of the $^4S_{3/2}$ state of earth has been altered (see supporting information Fig S1). XRD(Table1) results show that the cell volume decreased with increasing Co^{2+} ion doping(0-15mol% Co^{2+}) leading to the decrease in the average Ln^{3+}-Ln^{3+} bond length, indicating the distance between Er^{3+}-Er^{3+} or Yb^{3+}-Er^{3+} is decreased; on the contrary, the cell volume increased with increasing Co^{2+} ion doping(15-30mol% Co^{2+}) leading to the increase in the average Ln^{3+}-Ln^{3+} bond length, which result in the increase of the intensity of upconversion emission. Therefore, upconversion emission can be enhanced by adjusting the Co^{2+} ions codoping concentration and allowing precise control over the average ionic distance between the trivalent lanthanide dopants.

To verify the above results, the decay profiles of $^4S_{3/2}\rightarrow{}^4I_{15/2}$(541nm) and $^4F_{9/2}\rightarrow{}^4I_{15/2}$(657nm) transition in $NaYF_4$: Yb^{3+}/Er^{3+} nanoparticles with introducing 0-30 mol%Co^{2+} under the excitation of 980nm were measured. Fig.6 shows the distance between Er^{3+}-Er^{3+} or Yb^{3+}-Er^{3+}. As shown in Fig.S1, the surrounding environment of a certain point of Co^{2+} 15 mol% sample is the most asymmetric with the crystal structure analysis results. Asymmetric surrounding environment favours $NaYF_4$:Yb^{3+}/Er^{3+} NPs with different concentration of Co^{2+} ions were longer than that of $NaYF_4$:Yb^{3+}/Er^{3+} NPs without Co^{2+} ions, and the longest lifetime of the $^4S_{3/2}$ state was found in the sample codoping with 15 mol% Co^{2+} ions. Furthermore, the lifetimes had been prolonged after the Co^{2+} codoping and the similar changing trend of the enhancement of UC luminescence intensity was observed. The prolonged lifetimes might arise from the tailored local environment of Er^{3+} ions which was in close agreement with the experimental result shown in Fig.1S.

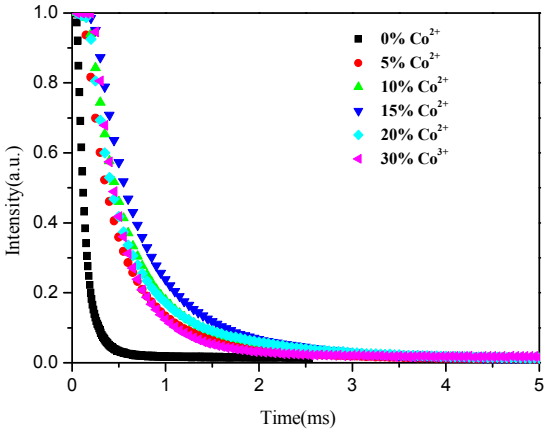

Fig. 6 Decay profiles of $^4S_{3/2}\rightarrow{}^4I_{15/2}$ transition in $NaYF_4$: Yb^{3+}/Er^{3+} NPs with introducing 0-30 mol%Co^{2+} under the excitation of 980nm.

3.3 Tunable magnetic behaviour

Besides the enhancement of the UC emission, the Co^{2+} codoped $NaYF_4$ NPs also present particular paramagnetic properties due to the weakly coupled and uncoupled of Co^{2+} ions. Fig.7 shows magnetization versus magnetic field (M-H) curves for $NaYF_4$ NPs codoped with different Co^{2+} contents measured at room temperature. The magnetization increased with increasing Co content, showed that all the samples present typical paramagnetic behaviour at room temperature indicating that the Curie temperature (Tc) of this material is below room temperature. The paramagnetic behaviour is mainly attributed to the seven unpaired inner 3d electrons, which are closely bound to the nucleus and effectively shielded by the outer closed shell electrons ($4s^23d^7$) from the crystal field.[28-32] The magnetic mass susceptibilities of the as prepared $NaYF_4$ nanocrystals doped with 5%, 10%, 15%, 20% and 30% Co^{2+} are 0.05, 0.06, 0.07, 0.08, 0.11emu g^{-1} Oe^{-1}, respectively. The magnetization of the $NaYF_4$ NPs can be modified from 0.30 emu.g^{-1} to 0.67 emu.g^{-1} at 6T with increasing the Co^{2+} doping content from 5mol% to 30mol%, which is close to the

previously reported value for bio-separation based on nanoparticles[33]. In addition, the *M(H)* values at 2 and 300K for Co^{2+} doped $NaYF_4$: Yb^{3+}/Er^{3+} NPs are shown in Fig S5. Typical superparamagnetism behaviour is observed at 2K due to the absence of remanence (Mr) or coercivity (Hc), and the saturation magnetization (Ms) is approximately 13.77emu/g for the sample of 30% Co^{2+} doped $NaYF_4$: Yb^{3+}/Er^{3+} NPs. These results indicate that these multifunctional NPs may have promising potential applications in bio-separation and magnetic resonance imaging.

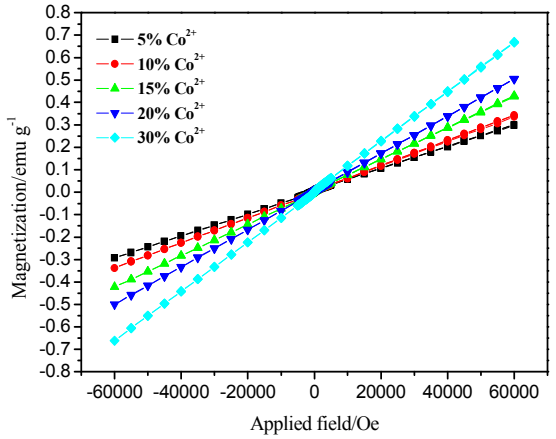

Fig. 7 Magnetization as a function of an applied field for $NaYF_4$: Yb^{3+}/Er^{3+} NPs codoped with different Co^{2+} ions concentration.

4. Conclusions

In conclusion, $NaYF_4$:Yb/Er NPs codoped with different concentration of Co^{2+} ions were first synthesized via a co-thermolysis method using oleic acid as capping ligand and octadecene as solvent. The results show that Co^{2+} ions codoping in $NaYF_4$:Yb/Er NPs did not change the hexagonal phase structure of naoparticles, and the size, morphology and dispersibility in nonpolar solvent were all maintained by codoping with Co^{2+} ions. However, the significant enhancement of the UC emission in $NaYF_4$: Yb^{3+}/Er^{3+} NPs by introducing Co^{2+} ions were observed. Visible green and red intensity of UC emissions in $NaYF_4$:Yb^{3+}/Er^{3+} NPs were enhanced by up to 114 and 84 times by introducing 15 mol% Co^{2+} ions, respectively. Furthermore, the Co^{2+} codoped $NaYF_4$:Yb^{3+}/Er^{3+} NPs also exhibit paramagnetic behavior at room temperature and extra paramagnetic behaviour at low temperature, which is familiar to the properties of Gd^{3+} doped $NaYF_4$:Yb^{3+}/Er^{3+} NPs. Therefore, the Co^{2+} codoping method not only enhances the intensity of UC emission to a large extent, but also incorporates additional magnetic functionality into these single phase fluorescent materials. Therefore, the synthesized composites may have potential application in in vitro and in vivo dual-modal fluorescent and magnetic bioimaging as well as bioseparation

Acknowledgements

This work was supported by the Fundamental Research Funds for the Central Universities (Grant No. 2572014CB08) ， The Natural Science Foundation of Heilongjiang Province (Grant No.E201404), Heilongjiang Province postdoctoral Science Foundation (Grant No. LBH-Z14004).

Notes and references

1 C. C. Mi, Z. H. Tian, C. Cao, Z. J. Wang, C. B. Mao and S. K. Xu, *Langmuir*, 2011, **27**, 14632..
2 Z. Q. Li, Y. Zhang and S. Jiang, *Adv Mater*, 2008, **20**, 4765.
3 H. S. Qian and Y. Zhang, *Langmuir*, 2008, **24**, 12123.
4 C. Renero-Lecuna, R. Marti´n-Rodri´guez, R. Valiente, J. Gonza´lez, F. Rodri´guez, K. W. Kra¨mer and H. U. Gu¨del, *Chem Mater*, 2011, **23**, 3442.
5 Q. Q. Dou and Y. Zhang, *Langmuir*, 2011, **27**, 13236.
6 C. Dong, A. Korinek, B. Blasiak, B. Tomanek and F. C. J. M. van Veggel, *Chem Mater*, 2012, **24**, 1297.
7 C. F. Gainer, G. S. Joshua, C. R. De Silva and M. Romanowski, *J Mater Chem*, 2011, **21**, 18530.
8 G. Y. Chen, T. Y. Ohulchanskyy, S. Liu, W. C. Law, F. Wu, M. T. Swihart, H. Agren and P. N. Prasad, *ACS nano*, 2012, **6**, 2969.
9 L. Cheng, C. Wang and Z. Liu, Nanoscale, 2013, 5, 23-37.
10 R. Deng and X. Liu, *Nat Photon*, 2014, 8, 10-12.
11 K. Prorok, A. Bednarkiewicz, B. Cichy, A. Gnach, M. Misiak, M. Sobczyk and W. Strek, *Nanoscale*, 2014, 6, 1855-1864.
12 F. Wang, Y. Han, C. S. Lim, Y. H. Lu, J. Wang, J. Xu, H. Y. Chen, C. Zhang, M. H. Hong and X. G. Liu, *Nature*, 2010, **463**, 1061.
13 H. J. Hao, M. Qin and P. Li, *J Alloy Compd*, 2012, **515**, 143.
14 F. Ahmed, S. Kumar, N. Arshi, M. S. Anwar, B. H. Koo and C. G. Lee, *Microelectron Eng*, 2012, **89**, 129.
15 R. Sarkar, C. S. Tiwary, P. Kumbhakar and A. K. Mitra, *Physica B*, 2009, **404**, 3855.
16 S. Han, R. Deng, X. Xie and X. Liu, *Angewandte Chemie International Edition*, 2014, 53, 11702-11715.
17 D. Yin, C. Wang, J. Ouyang, K. Song, B. Liu, X. Cao, L. Zhang, Y. Han, X. Long and M. Wu, *Dalton Trans*, 2014, 43, 12037-12043.
18 G. Tian, Z. Gu, L. Zhou, W. Yin, X. Liu, L. Yan, S. Jin, W. Ren, G. Xing, S. Li and Y. Zhao, *Adv. Mater.*, 2012, **24**, 1226.
19 D. Tian, D. Gao, B. Chong and X. Liu, *Dalton Trans*, 2015, 44(9): 4133-4140.
20 P. Ramasamy, P. Chandra, S. W. Rhee and J. Kim, *Nanoscale*, 2013, 5, 8711.
21 Q. Cheng, J. Sui and W. Cai, *Nanoscale*, 2012, 4, 779-784.
22 Q. M. Huang, J. C. Yu, E. Ma and K. M. Lin, *J. Phys. Chem. C*, 2010, **114**, 4719.
23 H. Yu, W. Cao, Q. Huang, E. Ma, X. Zhang and J. Yu, *Journal of Solid State Chemistry*, 2013, 207, 170-177.
24 D. Li, Y. Wang, X. Zhang, H. Dong, L. Liu, G. Shi and Y. Song, *J.Appl. Phys.*, 2012, **112**, 09470
25 A. Xia, X. Zhang, J. Zhang, Y. Deng, Q. Chen, S. Wu, X. Huang and J. Shen, *Biomaterials*, 2014,**35**, 9167.
26 P. Ramasamy, P. Chandra, S. W. Rhee and J. Kim, *Nanoscale*, 2013, 5, 8711-8717.
27 G. Dong, B. Chen, X. Xiao, G. Chai, Q. Liang, M. Peng, J. Qiu, *Nanoscale*, 2012,4,4658-4666.
28 W. H. Zhang, F. Ding and S.Y. Chou, *Adv Mater*, 2012. **24**(35): OP236.
29 R. Deng and X. Liu, *Nat Photon*, 2014, 8, 10-12.
30 A. Bandyopadhyay, S. Sutradhar, B. J. Sarkar, A. K. Deb and P. K. Chakrabarti, *Appl Phys Lett*, 2012, **100.**
31 D. Santos and M. A. Macedo, *Physica B*, 2012, **407**, 3229.

32 L. Hu, C. de Montferrand, Y. Lalatonne, L. Motte and A. Brioude, *J. Phys. Chem. C*, 2012, **116**, 4349.
33 S. Zeng, M. Tsang, C. Chan, K. Wong, B. Fei and J. Hao, *Nanoscale*, 2012, **4**, 5118.